Available online at www.sciencedirect.com
SCIENCE DIRECT
ELSEVIER
Nuclear Instruments and Methods in Physics Research A 527 (2004) 145–150
NUCLEAR INSTRUMENTS & METHODS IN PHYSICS RESEARCH Section A
www.elsevier.com/locate/nima

A modification of the dual energy window subtraction method for scatter compensation in pixelized scintillators for SPECT

G. Loudos[a,c], N. Sakelios[a,b], N. Giokaris[a,b,*], K. Nikita[a,c], N. Uzunoglu[a,c], D. Maintas[d]

[a] Institute of Accelerating Systems and Applications, P.O.Box 17214, Athens 10024, Greece
[b] National Capodistrian University of Athens, Panepistimiou 30, Athens 10679, Greece
[c] National Technical University of Athens, Iroon Polytexneiou 9, Zografos, Athens 15773, Greece
[d] Athens Medical Center Institute of Isotopic Studies, Distomou 5-7, Marousi, Athens 15125, Greece

Abstract

Small field of view detectors based on Position Sensitive Photomultiplier Tubes (PSPMTs) have been widely used by many research groups in small-animal imaging and recently clinically in scintimammography. In most cases the PSPMT is coupled to pixelized scintillators since it has been shown that their use improves spatial resolution. The use of a single energy window for each crystal element is the only proposed method for scatter correction in pixelized scintillators. In this work we have modified the dual energy window subtraction technique in order to be applicable to a pixelized scintillator detector and we have evaluated its performance with real data. Hot, cold and breast phantoms have been imaged in planar mode.

PACS: 87.58.Ce; 87.57.Ce; 29.40.Gx

Keywords: Scatter compensation; Dual energy window subtraction method; Pixelized scintillator; PSPMT

1. Introduction

The aim of scintigraphic and SPECT imaging is the quantitative determination of a radionuclide distribution that is present in the object to be imaged. Two areas of great research interest are small-animal imaging and scintimammography. Small animals are widely used in order to study radiopharmaceuticals that are under development. However, a detector suitable for small-animal imaging should be characterized by high spatial resolution and sensitivity [1]. Another application, where such dedicated imaging systems are required is the detection of small breast tumors [2].

Small gamma cameras based on Position Sensitive Photomultiplier Tubes (PSPMTs) [3] meet the requirements for this dedicated type of imaging. A number of such detectors with 1–2 mm spatial resolution in planar and SPECT mode have been constructed by several research groups [4–9]. A typical PSPMT camera is equipped with an array of scintillation crystals (NaI(Tl), CsI(Tl), YAP:Ce, etc.). Scintillator arrays are used for

*Corresponding author. Institute of Accelerating Systems and Applications, P.O. Box 17214, Athens 10024, Greece. Tel.: +30-1-725-7533; fax: +30-1-729-5069.
E-mail address: ngiokar@cc.uoa.gr (N. Giokaris).

0168-9002/$ - see front matter
doi:10.1016/j.nima.2004.03.112

photon detection since they produce very focused light spot depending on pixel size and crystal thickness thus improving spatial resolution [10].

The pixelization of the scintillator introduces the need for a more sophisticated signal analysis. A look up table (LUT) that maps each crystal area is necessary since the non-uniform response of the scintillator, the PSPMT and amplification electronics introduce spatial distortions in the calculation of the position of the center of each incident photon. Calibration steps and energy corrections can be performed in a pixel level, since the LUT allows the construction of an energy spectrum for each crystal cell [11–13].

Thus an energy window is applied around the photopeak channel of each crystal in order to exclude Compton scattered photons, which carry inaccurate energy and mainly spatial information. Most groups working with PSPMT detectors use this method for scatter rejection [14]. However, this technique cannot exclude scattered photons with energy that appears to be in the photopeak window due to the poor energy resolution and physical parameters [15]. Monte-Carlo simulations have shown that a significant number of scattered photons are included in the primary photopeak window. In addition there is a lower region of the energy spectrum before the photopeak where most of the photons are scattered. Although these photons may have a different scatter cause than the photopeak scattered photons they can be used in order to provide an estimation of the scattered quantity that is included in the primary photopeak window [16].

Jaszczak et al. proposed a dual energy window subtraction technique (DEWST) for scatter correction [17,18]. Data are collected both in the primary and a lower energy window. Then the lower energy window data are multiplied with a weighting factor k and are subtracted from the photopeak data. If P is the photopeak image and L the lower energy window image then the corrected image C can be calculated as $\mathrm{C} = \mathrm{P} - k \cdot \mathrm{L}$. When the method is applied to conventional gamma cameras the two windows for ^{99m}Tc are usually around 127–153 and 92–125 KeV, respectively. The value of factor k is determined by Monte-Carlo simulations and approximates 0.5 [19–21].

In this work this technique has been applied by using the energy spectrum of each crystal element. Since a Monte-Carlo simulation is under development [22] and the energy response of each pixel varies the lower energy window was determined experimentally.

2. Methods

2.1. Data acquisition system

The gamma camera consists of a PSPMT (Hamamatsu R2486) and a pixilated CsI(Tl) scintillator. The spatial resolution of the system has been measured and found <2 mm in planar imaging [23]. The crystal is 4.6 cm in diameter, 4 mm thick and cells size is $1.13 \times 1.13\,\mathrm{mm}^2$. The camera is equipped with a 2.75 cm thick collimator with parallel hexagonal holes ~ 1.1 mm in diameter, with a 0.25 mm septa. The 16 anode signals are preamplified and then transferred to a CAMAC system. The digital signals are transported to a G3 Power Mac via a SCSI bus.

Acquisition software is written in $K_{\max}$ 6.4.5. (Sparrow Corporation) environment. Data have been acquired in a 100% energy window and stored in files event by event. The files have been post-processed using specific software that allows image reconstruction in several lower energy windows and the implementation of the DEWST for several k values. When the optimum k value and lower energy windows are determined the method can be applied in real time.

2.2. Phantom data

In order to simulate a non-scatter geometry a capillary 1.1 inner diameter filled with a ^{99m}Tc solution has been placed 8 cm from the center of the detector. The same capillary was placed in the center of a 16 cm water filled cylindrical pot in order to estimate the effects of scattering. A hot, a cold and a breast phantom have been used in order to evaluate the method in several imaging cases.

The hot phantom consists of three capillaries 7 cm long, with 1.5 mm inner diameter and 1.6 mm outer diameter, placed in 5 and 6.5 mm distances from each other and filled with a ^{99m}Tc solution (8 mCi/ml). The phantom was placed in a 10 cm distance from the collimator and a pot filled with 300 ml of water was placed as described above, between the phantom and the detector. The phantom was imaged for 150 s and ~301 K counts were acquired.

The cold phantom was a metallic cylinder 1.5 cm inner diameter, 0.8 cm outer diameter and 0.7 cm in height placed in the bottom of a thin plastic pot, 6 cm in diameter and 8 cm high. The pot was filled with 30 ml of a ^{99m}Tc solution 0.14 mCi/ml. The detector was placed in a 10 cm distance from the bottom of the pot. The phantom was imaged for 3 min and ~600,000 counts were acquired.

The breast phantom consists of two hot quantities of a ^{99m}Tc solution, 0.5 ml in volume, placed under a pot, 10 cm in diameter, containing a 300 ml ^{99m}Tc solution 2 mCi/ml. The activity ratios of the spot to the background were 5 : 1 and 10 : 1. The detector was placed in a 10 cm distance from the bottom of the pot. The phantom was imaged for 16 min and ~790,000 counts were collected.

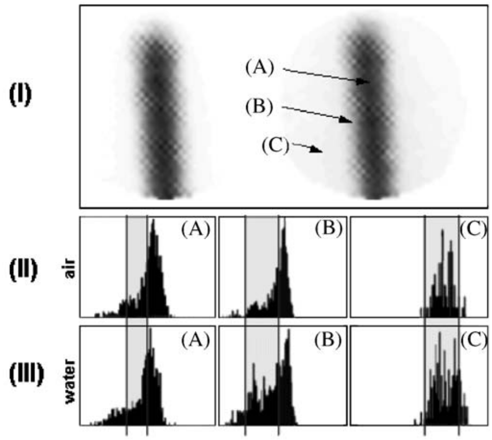

Fig. 1. (I) Two images of a capillary filled with a 99 mTc solution. Left: Image when the capillary is placed in the air in 8 cm distance from the collimator. Right: Image when the capillary is placed in the center of a cylinder 16 cm in diameter filled with water in order to study scatter effects. Comparison of the energy spectrums in typical crystal pixels in regions A, B and C, marked in (I), when the capillary is (II) in the air, and (III) when water is present. The regions of the spectrums where significant changes are observed are shaded.

2.3. Selection of lower energy windows and k factor

The capillary phantom has been imaged both in the air and in the water as described above and the two resulting images are shown in the upper part of Fig. 1. In order to study the effect of the presence of water that acts as a scattering medium, three regions have been investigated in order to observe differences in the spectrum. The first (A) corresponds to pixels in the capillary region, the second (B) to pixels in an intermediate region and the third (C) to pixels in the background region. In the lower part of Fig. 1 the energy spectrums of typical pixels in these regions are compared both in the air and in water. The regions of the spectrums where significant changes were observed are shaded.

This change is more noticeable in region B that lies above the edges of the capillary. In this region the total number of photons in a lower energy window is increased and we assume that the main reason for that is scattering. However, the width of the energy windows where these differences are observed vary from pixel to pixel and it also depends on the position of the pixel with respect to the object to be imaged. In general, the smallest width is in case (A) and the largest in case (C). Since in an experimental situation it is not possible to know in which region each pixel is located one optimum window should be determined and applied to all pixels.

For this reasons we have tested 10 possible energy windows with different central channels and widths, which are located before or near the photopeak channel. In some windows, part of the photopeak is included as well, in order to investigate the contribution of Compton scattered photons that are found in the lower portion of the photopeak [24]. The center and the width of the windows are expressed as a percentage of the photopeak channel.

In order to find the window that contains the maximum scatter information ten images of the capillary phantom in water have been constructed for each of these windows. Line profiles were drawn in the center of the images, which have shown that the $65 \pm 5\%$ window provided the lowest source to background ratio and the highest contrast. In addition the image from photons in this window looks more blurred compared to the images in the other lower energy windows, thus it is selected as the optimal lower energy window.

In order to determine factor k, the $65 \pm 5\%$ image was multiplied with several values of k ranging from 0.40 to 0.65 and then subtracted from the image in the 20% photopeak window. The shapes of the profiles at the tails of the photopeak were compared and the resulting image that provided the closest results to the air photopeak image was selected. The difference between these two images was minimized when $k = 0.5$. Higher k values, although they improved image contrast, overestimated the scatter component and introduced negativities in the image with no physical meaning [25].

3. Results

3.1. Hot phantom

In the case of the hot phantom, the presence of water increases image background and decreases resolution. In Figs. 2a and b the image in a $\pm 20\%$ photopeak window and the scatter corrected image using the DEWST and a $(65 \pm 5)\%$ lower energy window are shown, respectively. In Fig. 2c normalized line profiles across the capillaries have been drawn. The profiles are 41 pixels long and 3 pixels wide in order to have an average of more crystal cell.

The application of the DEWST results in improved image contrast, as it can be seen in the line profiles. In the line profiles of the three capillaries, the method seems to increase the spatial resolution of the system.

3.2. Cold phantom

In the case of the cold phantom, where the effects of scattering are more significant, the application of the DEWST improves contrast. In Figs. 3a and b the image in a $\pm 20\%$ photopeak window and the scatter corrected image using the DEWST and a $65 \pm 5\%$ lower energy window are shown, respectively. In Fig. 3c normalized line profiles across the center of the cylindrical cold phantom have been drawn.

3.3. Breast phantom

In Fig. 4 the images of a simple breast phantoms are shown. In Figs. 4a and b the image in a $\pm 20\%$ photopeak window and the scatter corrected image using the DEWST and a $65 \pm 5\%$ lower energy window are shown, respectively. In Fig. 4c normalized line profiles 41 pixels long and 3 pixels wide across the centers of the two hot spots have been drawn.

The scattered corrected images with the proposed method have a lower background and an improved image contrast. As it can be derived

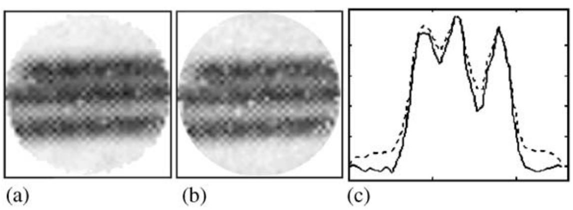

Fig. 2. Images of a hot phantom consisting of 3 capillaries filled with a 99 mTc solution. The phantom is placed under a pot filled with water. (a) The image in a $\pm 20\%$ photopeak window, (b) the scatter corrected image using the DEWST with a $65 \pm 5\%$ lower energy window and $k = 0.5$, and (c) normalized line profiles. The dashed line corresponds to the photopeak image and the solid line to the scattered corrected image.

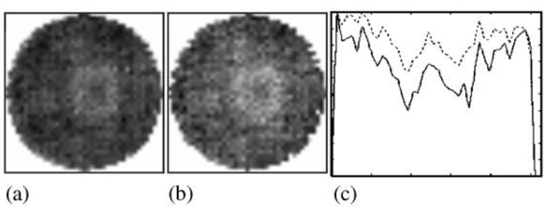

Fig. 3. Images of a cold phantoms consisting of a metallic cylinder placed in a pot filled with a 99 mTc solution. (a) The image in a $\pm 20\%$ photopeak window, (b) the scatter corrected image using the DEWST with a $65 \pm 5\%$ lower energy window and $k = 0.5$, and (c) normalized line profiles. The dashed line corresponds to the photopeak image and the solid line to the scattered corrected image.

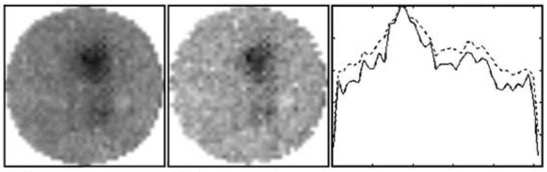
(a) (b) (c)

Fig. 4. Images of a breast phantoms described in 2.2. (a) The image in a $\pm 20\%$ photopeak window, (b) the scatter corrected image using the DEWST with a $65 \pm 5\%$ lower energy window and $k = 0.5$, and (c) normalized line profiles through the centers of the spots. The dashed line corresponds to the photopeak image and the solid line to the scattered corrected image.

from the line profiles, the hot spot with activity ratio to the background 5:1 can be better separated when the DEWST is applied. In addition the edges of the hot spots are sharper in the case of the scattered corrected images thus their shape can be better determined.

4. Discussion/conclusion

Scatter correction in pixelized detectors is mainly performed by applying an energy window around the photopeak channel of each crystal. However, this method cannot reject scattered photons that are included in the primary photopeak window. The DEWST has been applied in conventional SPECT systems by a number of authors using the energy spectrum of the system [15–21]. In order to apply the method in a pixilated crystal we have used the energy spectrum of each crystal cell. The modified DEWST has been applied to a number of hot, cold and breast phantoms providing improved results when compared with the standard use of one photopeak window.

The energy spectrum of each crystal cell is affected by the non-uniformities of the system, thus the center and the width of the optimum lower energy window are calculated as a percentage of the photopeak channel, which is refreshed during the calibration procedures. Instead of using a capillary in the air and in water in order to provide system line response function in scatter-free and scatter conditions, respectively, a point source in the air and water can be used. The Monte-Carlo simulation of the system [22], will be used for the exact determination of the optimum lower energy window and the results will be compared with those that have been obtained with the experimental approach.

The suggested values offer best results in the existing small field of view gamma camera that was used, in a large number of phantom studies, which have been performed over a period of more than one year. These values characterize our system but in another system the best lower energy window and k value might differ. Thus a similar procedure should be followed in order to determine the optimum parameters for the application of DEWST. The value of k may also depend on the source depth inside the absorbing-scattering medium and this has to be investigated as well.

The results from breast phantoms imaging indicate that this technique could be helpful for scatter rejection in scintimammography with dedicated systems based on PSPMTs [26–29]. The presented technique could enhance scintimammography images and allow the exact localization of small tumors. The evaluation of the method with data from anthropomorphic phantoms and clinical data are necessary in order to investigate the benefits from this technique.

Other scatter correction techniques that have been proposed for conventional SPECT systems can be modified and implemented in the level of a crystal cell. The multiple energy windowed subtraction technique [20,30] and the deconvolution subtraction technique [31] are now being evaluated providing very encouraging results that will be compared with the results from DEWST. In addition the performance of these techniques will be explored in SPECT mode as well. Finally similar modifications of scatter correction methods could be performed for other pixilated detectors like semiconductor detectors [32,33].

Acknowledgements

This work has been partly supported by the Greek General Secretariat for Research and Technology (GGET) and by EEC RTN contract

HPRN-CT-00292-2002. The authors would like to thank S. Majewski and A. Weisenberger of "Jefferson's lab" and R. Pani and F. Scopinaro of the University of Rome "La Sapienza" for offering part of the used equipment.

References

[1] M.V. Green, J. Seidel, J.J. Vaquero, E. Jagoda, I. Lee, W.C. Eckelman, Comput. Med. Imag. Graphics 25 (2001) 79.
[2] J. Maublant, Eur. J. Radiol. 24 (1997) 2.
[3] Hamamatsu Technical Data Sheets, supersedes, October 2000.
[4] R. Pani, R. Pellegrini, F. Scopinaro, et al., Nucl. Instr. and Meth. A 392 (1987) 295.
[5] A.G. Weisenberger, S. Majewski, M. Saha, E. Bradley, Nucl. Instr. and Meth. A 392 (1997) 299.
[6] A.G. Weisenberger, E. Bradley, S. Majewski, M. Saha, IEEE Trans. Nucl. Sci. NS-145 (3) (1998) 1743.
[7] N. Schramm, A. Wirrwar, H. Halling, IEEE Trans. Nucl. Sci. NS-47(3) Part 3 (2000) 1163.
[8] J.H. Kim, Y. Choi, K.S. Joo, B.S. Sihn, J.W. Chong, S.E. Kim, K.H. Lee, Y.S. Choe, B.T. Kim, Phys. Med. Biol. 45 (11) (2000) 3481.
[9] G.K. Loudos, K.S. Nikita, N.D. Giokaris, E. Styliaris, S.C. Archimandritis, A.D. Varvarigou, C.N. Papanicolas, S. Majewski, D. Weisenberger, R. Pani, F. Scopinaro, N.K. Uzunoglu, D. Maintas, K. Stefanis, Appl. Radiat. Isotopes 58 (4) (2003) 501.
[10] R. Pani, R. Pellegrini, A. Soluri, G. De Vincentis, R. Scafe, A. Pergola, Nucl. Instr. and Meth. A 409 (1–3) (1998) 524.
[11] F. Vittori, F. de Notaristefani, T. Malatesta, D. Puertolas, Nucl. Instr. and Meth. A 452 (2000) 245.
[12] F. Vittori, T. Malatesta, F. de Notaristefani, Nucl. Instr. and Meth. A 418 (1998) 497.
[13] R. Pani, R. Scafè, R. Pellegrini, A. Soluri, G. Trotta, L. Indovina, M.N. Cinti, G. De Vincentis, Nucl. Instr. and Meth. A 477 (1–3) (2002) 72.
[14] A. Weisenberger, M. Williams, R. Wojcik, S. Majewski, F. Farzanpay, A. Goode, B. Kross, D. Steinbach, Nucl. Instr. and Meth. A 409 (1998) 520.
[15] B. Axelsson, P. Msaki, A. Israelsson, J. Nucl. Med. 25 (1984) 490.
[16] L. Shao, R. Freifelder, J.S. Karp, IEEE Trans. Med. Imag. 13 (4) (1994) 641.
[17] R.J. Jaszczak, K.L. Greer, C.E. Floyd, C.C. Harris, R.E. Coleman, J. Nucl. Med. 29 (1984) 893.
[18] R.J. Jaszczak, C.E. Floyd, R.E. Coleman, IEEE Trans. Nucl. Sci. NS-32 (1985) 786.
[19] J.C. Yanch, M.A. Flower, S. Webb, Med. Phys. 17 (6) (1990) 1011.
[20] M.C. Gilardi, V. Bettinardi, A. Todd-Pokropek, L. Milanesi, F. Fazio, J. Nucl. Med. 29 (12) (1988) 1971.
[21] J.W. Beck, R.J. Jaszczak, R.E. Coleman, C.F. Starmer, L.W. Nolte, IEEE Trans. Nucl. Sci. NS-29 (1982) 506.
[22] D. Lazaro, I. Buvat, G. Loudos, D. Strul, G. Santin, N. Giokaris, D. Donnarieix, L. Maigne, V. Spanoudaki, S. Styliaris, S. Staelens, V. Breton, Phys. Med. Biol. 49 (2004) 271.
[23] G.K. Loudos, K.S. Nikita, N.K. Uzunoglu, N.D. Giokaris, C.N. Papanicolas, S.C. Archimandritis, A.D. Varvarigou, D. Maintas, Comput. Med. Imag. Graphics 27 (4) (2003) 307.
[24] M.A. King, G.J. Hademenos, S.J. Glick, J. Nucl. Med. 33 (4) (1992) 605.
[25] G. Loudos, N. Sakelios, K. Nikita, N. Giokaris, N. Uzunoglu, D. Maintas, Comput. Med. Imag. Graphic, (2004) in press.
[26] S. Majewski, E. Curran, C. Keppel, D. Kieper, B. Kross, A. Pulumbo, V. Popov, A.G. Weisenberger, B. Welch, R. Wojcik, M.B. Williams, A.R. Goode, M. More, G. Zang, IEEE Trans. Nucl. Sci. NS-48 (3) (2001) 822.
[27] R.F. Brem, J.M. Schoonjans, D.A. Kieper, S. Majewski, S. Goodman, C. Civelek, J. Nucl. Med. 43 (2002) 909.
[28] R. Pani, A. Soluri, R. Scaf, R. Pellegrini, A. Tat, F. Scopinaro, G. De Vincentis, T. Gigliotti, A. Festinesi, F. Garibaldi, A. Del Guerra, Nucl. Instr. and Meth. A 477 (2002) 509.
[29] G. De Vincentis, F. Scopinaro, R. Pani, R. Pellegrini, A. Soluri, R. Scafè, R. Massa, M.N. Cinti, I.N. Weinberg, I. Khalkhali, M. Betti, Nucl. Instr. and Meth. A 497 (1) (2003) 46.
[30] A.E. Todd-Pokropek, G. Clarke, R. Marsh, in: F. Decknonic (Ed.), Information Processing in medical Imaging, Martinus Nijhoff Publishers, Bruxelles, 1983, pp. 130–150.
[31] C.E. Floyd, R.J. Jaszczak, K.L. Greer, R.E. Coleman, J. Nucl. Med. 26 (4) (1985) 403.
[32] H.B. Barber, Nucl. Instru. and Meth. A 436 (1999) 102.
[33] G.A. Kastis, M.C. Wu, S.J. Balzer, D.W. Wilson, L.R. Furenlid, G. Stevenson, H.B. Barber, H.H. Barrett, J.M. Woolfenden, P. Kelly, M. Appleby, IEEE Trans. Nucl. Sci. NS-49 (1) (2002) 172.